Characterization of Grain Boundary Disconnections in $SrTiO_3$

Part II: The Influence of Superimposed Disconnections on Image Analysis

Hadas Sternlicht[1,*], Wolfgang Rheinheimer[2,**], Judy Kim[3,4], Emanuela Liberti[3,4], Angus I. Kirkland[3,4], Michael J. Hoffmann[5], and Wayne D. Kaplan[6]

[1] School of Engineering, Brown University, Providence, USA.

[2]Purdue University, Materials Engineering, West Lafayette, USA

[3]Department of Materials, University of Oxford, Parks Road, Oxford, OX1 3PH, United Kingdom

[4] Electron Physical Sciences Imaging Centre, Diamond Lightsource Ltd., Diamond House, OX11 0DE, United Kingdom

[5]Karlsruhe Institute of Technology, Institute of Applied Materials, Karlsruhe, Germany.

[6]Department of Materials Science and Engineering, Technion – Israel Institute of Technology, Haifa, Israel.

[*]Conducted when the author was at (6)

[**]Conducted when the author was at (5)

Abstract

Disconnections were recently shown to play a role in the mechanism of grain boundary motion in general grain boundaries in $SrTiO_3$. In this work, we demonstrate the existence of disconnections in the viewing direction along the projected thickness of transmission electron microscopy samples and characterize possible aspects of the structure of these disconnections. We show that the presence of steps along the viewing direction may result in the appearance of a disordered region at the boundary, while it is actually composed of ordered crystalline material. We discuss the subsequent complications in analysis of transmission electron microscopy data and strict meaning of the term "edge-on" for grain boundaries.

Introduction

Modern high resolution transmission electron microscopy (HRTEM) is important when characterizing structural defects due to its ability to achieve real space sub-Angstrom resolution with reduced contrast delocalization for relatively straightforward interpretation of image contrast at extended defects. The latter can be achieved using negative spherical aberration (Cs) imaging conditions combined with exit wave reconstruction [1].

Negative Cs conditions provide bright intensity in HRTEM micrograph directly correlated with the position of atomic columns, in addition to minimization of the contrast delocalization [1,2]. Exit wave reconstruction recovers the complex wave function at the exit plane of the sample, offering additional advantages for quantitative analysis. These advantages include an enhanced

signal to noise ratio compared to single micrographs, removal of residual contrast delocalization and the measurement of residual aberrations a posteriori and the removal of non-linear imaging artifacts. In addition, no information is lost due to null contrast at specific spatial frequencies, which is intrinsic to a single experimental micrograph due to the form of the phase contrast transfer function [3,4,5,6,7].

As a result, structural information can be recovered at resolutions beyond those achieved using conventional imaging (which are limited by the temporal and spatial coherence of the incident wave). The required data sets needed for exit wave reconstruction are either defocus series of HRTEM micrographs or a tilted illumination series of HRTEM micrographs. Exit wave reconstruction performed using focal series is resolution limited by the coherence of the incident wave, whereas using tilt series, the resolution can be further extended [8,9]. Since exit wave reconstruction restores the complex wave function, free of the objective lens aberration, a comparison between simulated and experimental wave functions requires only one unknown parameter (the thickness), in contrast to a number of unknown variables involved when analyzing conventional HRTEM micrographs [5,8,9,10,11,12].

Exit wave reconstruction can be conducted using linear filters, such as the Wiener filter [5,7] or non-linear iterative methods [13,14,15]. In this work, we used the focal and tilt series restoration (FTSR) software [16] for general grain boundaries. As described elsewhere [17,18] FTSR initially uses a Phase Correlation Function to find the relative defocus values between images in a focus series and the image registration vectors, and subsequently a Phase Contrast Index Function to determine the absolute astigmatism and defocus. Finally, a linear Wiener filter is used to restore the exit wave function [19].

Recently, general high-angle grain boundaries in $SrTiO_3$ were shown to be composed of steps and microscopic segments of grain boundary planes, creating overall macroscopic (vicinal) grain boundary planes [20]. It was shown that in samples annealed under a relatively high oxygen partial pressure, the grain boundary and step planes were aligned mainly parallel to {001} and {110} crystallographic planes. These steps include a dislocation character creating overall disconnections [20].

In the present work, we have characterized the structure of these disconnections at general grain boundaries in $SrTiO_3$ annealed under a relatively high oxygen partial pressure, focusing on the structure of the macroscopic grain boundary planes along the viewing direction of the TEM samples, using aberration corrected TEM and exit wave reconstruction. General grain boundaries have been studied in either polycrystalline $SrTiO_3$ samples or as boundaries between a single crystal of $SrTiO_3$ of a predefined orientation diffusion bonded to polycrystalline $SrTiO_3$.

The kinetic behavior of the characterized grain boundaries was studied by Rheinheimer et al. who showed that a significant change in the grain boundary mobility appeared in a temperature range of 1350-1425°C in both polycrystalline $SrTiO_3$ and in diffusion bonded samples annealed under a relatively high oxygen partial pressure [21,22]. Thus, the present work will focus on samples annealed within this temperature range.

Experimental Methods

$SrTiO_3$ Samples

Two different sample types were used in the present study; standard polycrystalline samples and single crystals which were diffusion bonded to a polycrystal. For the polycrystals stoichiometric ceramic powder was prepared by a mixed oxide/carbonate route based on high purity raw materials ($SrCO_3$ and TiO_2, purity of 99.95% and 99.995%, Sigma Aldrich Chemie GmbH, Taufkirchen, Germany). Details of the synthesis are published elsewhere [23]. The green bodies were pre-sintered at 1425°C for 1 h in oxygen to obtain a relative density of 99.5±0.2 %. After pre-sintering, polycrystalline samples were heated at 20K/min to 1350°C and 1550°C in oxygen or air. For all heat treatments in this study, a tube furnace was used (Carbolite Gero GmbH & Co. KG, Neuhausen, Germany). After different heating times, samples were either furnace cooled, air-quenched, or water-quenched. For air quenching, the samples were removed from the hot zone of the furnace without changing the atmosphere yielding a cooling rate of more than 200 K/min. For water-quenching, samples were dropped into liquid water without changing the atmosphere. Cooling below 100°C was estimated to occur within 3 sec [20].

For the joining of diffusion bonded samples, pre-sintered polycrystals were cut into discs and polished (diamond slurry, 0,25 µm). The $SrTiO_3$ single crystals (impurity content: <10 ppm Si, <2 ppm Ba, <1 ppm Ca, SurfaceNet GmbH, Rheine, Germany) were chemical-mechanical polished and placed between two polished and intentionally scratched polycrystalline discs. Stacks were joined at 1430°C for 20 min in air with a compressive load of 1 MPa. More details of this procedure can be found elsewhere [20,22,24].

In a similar manner to the polycrystals, the diffusion bonded samples were heated to temperatures between 1350°C and 1425°C in oxygen. All diffusion bonded samples were water-quenched as described above.

Characterization Methods

TEM samples were prepared using the following methods:

a) The conventional method used was based on slicing, mechanical thinning, dimpling, and ion milling with Ar at 2-5kV, for polycrystalline samples.
b) The lift-out technique using a dual beam focused ion beam (FIB; FEI Strata 400s) was used for selecting and preparing TEM samples from the diffusion bonded samples, focusing on boundaries between the single crystal and a grain from the polycrystalline side [25].

The samples were characterized using an aberration corrected TEM (FEI Titan 80-300 keV S/TEM) operated at 300 keV. Each boundary was tilted to the edge-on condition, such that the electron beam was parallel to the macroscopic grain boundary plane.

Results

Recently, the existence of steps along edge-on general grain boundaries in $SrTiO_3$ was demonstrated using HRTEM [20]. For a boundary oriented to the edge-on condition, both the step and the grain boundary planes are parallel to the electron beam direction across the entire projected thickness of the sample (Figure 1a). At the same time, steps in the viewing direction of the TEM samples (in the direction of the projected thickness) are also expected to exist. Such steps in the viewing direction would shift the position of sections of the edge-on grain boundary plane in the viewing direction (Figure 1b). The steps in the viewing direction (the direction of the projected thickness of the sample) are defined in here as “inclined steps” since they are inclined to the viewing direction (the electron beam direction) to differentiate them

from “edge-on steps” which are parallel to the viewing direction. The existence of steps in the viewing direction of the TEM sample results in small changes in the position of the edge-on macroscopic grain boundary plane (which is composed of edge-on steps and grain boundary planes) in the viewing direction of the sample, as demonstrated schematically in Figure 1c. As such, the majority of the boundary is edge-on and the inclined steps are the only section of the macroscopic grain boundary plane which is tilted from the viewing direction.

In constructing Figure 1b,c we have assumed that in the majority of cases the segments of the grain boundary plane in the viewing direction are aligned parallel to the electron beam direction and the steps in the viewing direction are inclined. This assumption is consistent with our experimental data (as will be discussed below) since the artifacts resulting from the disconnections in the viewing direction are rather narrow and can be related to the shorter sections of the macroscopic grain boundary plane, meaning the steps. These cause small shifts in the position of sections of the grain boundary plane in the viewing direction, resulting in the projection of such inclined steps in the TEM micrograph to appear as narrow regions of indeterminate contrast. If the grain boundary plane was not parallel to the viewing direction (and the steps in the viewing direction were edge-on), the grain boundary plane in the viewing direction would be tilted and its projection would appear as wide regions of indeterminate contrast. As such, throughout the paper, we adopt the geometry of inclined steps rather than inclined grain boundary plane segments. It should however be considered that both possibilities can occur depending on the local curvature of the grain boundary and the one adopted here is that experimentally identified. In cases where the grain boundary and step planes are of similar length, this description would no longer be valid.

Noting the anisotropic nature of the edge-on steps and grain boundary planes in samples annealed under similar conditions [20], we expect the step and grain boundary planes in the viewing direction to be parallel to the same crystallographic planes. This assumption will be subsequently supported using simulations and experimental data. The description of the boundaries shown previously [20] represent the projections of samples with several inclined steps along the sample projected thickness, since the step and grain boundary planes are significantly smaller than the thickness of the samples.

As a result of inclined steps, the position of the edge-on step and grain boundary planes in Figure 1c is shifted by a certain distance normal to the edge-on step plane, normal to the edge-on grain boundary plane and in the direction of the electron beam. The distance of the resulting shift in the direction normal to the edge-on step and grain boundary planes is a projection of the length of the inclined step in these directions. In the direction of the electron beam, this distance is a projection of the length of the inclined step along the electron beam direction.

The presence of inclined steps is demonstrated in Figure 2, Figure 3, Figure 4 and Figure 5. The grain boundary and step planes were identified by the bright contrast in the HRTEM micrographs, even though the exact atomic arrangement cannot be determined (as described in detail in [26]). To distinguish between edge-on grain boundary and step planes and inclined steps, the edge-on planes were identified by bright contrast in the boundary region with a small decrease in intensity compared to the bulk. Inclined steps were thus identified by weaker contrast along the boundary region.

In the region of the micrograph showing inclined steps (or grain boundary planes), the lattice of one grain overlaps with that of the second grain, and a superimposed lattice pattern of the

two grains must then form. For example, Figure 2 presents a HRTEM micrograph of a polycrystalline sample, annealed at 1350°C for 10h in oxygen and quenched in gas, and then annealed at 1350°C in air and quenched in water. The dashed yellow lines indicate an area in the upper grain which is superimposed with the lower grain, presumably due to inclined steps. The inclined steps in this case would be perpendicular to the incident beam direction. As a result, the shifts between the positions of segments of grain boundary planes in the viewing direction are the inclined step height (or an integer multiple). As can be seen in Figure 2, these shifts match the length of an edge-on step. In addition, it is apparent that grain boundary planes and steps indicated by the dashed lines lay parallel to the yellow lines representing edge-on grain boundary and step planes. These findings support the assumption that the segments of the grain boundary plane in the viewing direction are parallel to the edge-on grain boundary planes and that the inclined steps are perpendicular to the edge-on grain boundary and step planes, such that the edge-on step and grain boundary planes and those in the viewing direction run parallel to the same family of crystallographic planes (are of the same nature).

In high angle annular dark field (HAADF) scanning transmission electron (STEM) micrographs from the same boundary (Figure 3), a decrease in intensity (compared to the bulk of the lower grain) is evident at the last planes of atoms which show the same periodicity as the lower grain. These planes are marked by the dashed yellow lines and are parallel to the edge-on step and grain boundary planes along the boundary marked by the yellow lines. In HAADF-STEM micrographs the contrast is dependent on the atomic number of the atoms in projection. Since the entire sample is composed of $SrTiO_3$, the decrease in intensity in the last planes of the lower grain must be correlated to a local decrease in the relative thickness of this grain in the sample. Since the overall thickness of the sample is relatively uniform (which was confirmed by electron energy loss thickness maps), the decrease in thickness of the lower grain

is due to the presence of inclined steps. As mentioned above for Figure 2, the shifts in the position of segments of grain boundary planes (distances between parallel yellow lines and dashed yellow lines) equals the length of an edge-on step. This, in addition to the dashed yellow lines being parallel to the edge-on step and grain boundary planes, supports the presence of inclined steps, which are of the same nature as the edge-on steps. The appearance of contrast resulting from inclined steps in HAADF-STEM micrographs is consistent with the contrast observed in HRTEM micrographs and the presence of inclined steps.

The dashed lines in Figure 2, Figure 3, Figure 4 and Figure 5 indicate regions with a relatively high density of inclined steps. Thus in HRTEM micrographs the superimposed lattice structure from the two grains is imaged. In areas with a lower density of inclined steps, marked by arrows in Figure 4 and Figure 5, only small parts that show this contrast are visible. Figure 4 presents a HRTEM micrograph of another boundary from the same sample from which Figure 2 was acquired. Figure 5 presents a HRTEM micrograph of a polycrystalline sample that was annealed at 1350°C for 10hr in oxygen and furnace cooled. In this case, a weak pattern of single or multiple spots which should not appear in the absence of inclined steps, are apparent. In Figure 4 these spots appear with the same periodicity as the lower grain “inside” the area related to the upper grain. These spots appear in the form of triangular patterns; indicated by the dashed lines in Figure 5. These features result from local changes in the relative thickness of each of the grains due to the presence of inclined steps. As such, the lattice contrast changes locally and the expected bulk four-fold symmetry is distorted to a triangular shape. In the HAADF-STEM micrographs (Figure 3) no triangular features were observed. This is due to the contrast in HAADF-STEM being less sensitive to small changes in effective thickness than phase contrast HRTEM imaging. This further supports our hypothesis that the appearance of triangular shaped features is due to inclined steps rather than actual changes in the atomistic

structure or strain. In these cases, due to the presence of inclined steps, there is no abrupt change in the contrast from one grain to the other. The periodicity of both types of artifacts (marked by dashed lines and arrows) indicate that the inclined steps are of the same nature as the edge-on step and grain boundary planes.

In order to detect grain boundary steps, the grain boundary must be aligned such that the majority of the boundary is edge-on, and the inclined steps are the only planes along the macroscopic grain boundary plane which are not edge-on. When the boundary is not aligned in such a manner, the projection of the boundary area is characterized by a relatively wide boundary region having a combination of moiré contrast, superimposed lattice patterns from the two grains and interference lines resulting from extinction distance. This will be subsequently defined as a "tilted boundary" in this work. In Figure 6 a HRTEM micrograph from a tilted boundary is presented, acquired from a polycrystalline $SrTiO_3$ sample that was annealed at 1350°C for 10h in oxygen, and quenched in gas at a cooling rate of ~200°C/min, then annealed again at the same temperature in air for an hour and finally quenched in water. Two lines of dark contrast appear along the boundary, apparently resulting from interference lines correlated to the extinction distance, since when the boundary is tilted the electron beam travels through varying distances in each of the grains in this region. The gradual change in the relative thickness of both grains can be described using the extinction distance, resulting in the appearance of dark and bright fringes [27]. The spacing between the dark lines is ~2.5nm. The fact that these dark lines are not straight supports our model for steps at the boundary. In Figure 6 an angle of ~137° was measured between the yellow lines. The yellow lines represent estimated planes for edge-on grain boundary and step planes (which would appear as edge-on planes after tilting the boundary such that the majority of the boundary is edge-on). One of these planes is the (011) plane in the upper grain. Based on a previous study [20], assuming

that the second plane is the $\left(00\bar{1}\right)$ plane in the upper grain, an angle of 135° is expected. A moiré pattern appears along the black lines (marked by red lines in Figure 6) with a measured periodicity of 0.87 nm matching the calculated spacing of the moiré pattern resulting from the (011) periodicities in each of the grains [27]. The direction of the expected moiré pattern resulting from the (011) planes of both grains is marked by a purple line in Figure 6. This line is in a similar direction to the red lines in the micrograph which indicate the moiré pattern. Between the black lines, superimposed lattice patterns from the two grains are evident. The appearance of step and grain boundary planes in a tilted boundary was noted in each of the studied boundaries *before* they were aligned such that the majority of the boundary was edge-on, regardless of the annealing temperature, quenching rate and the orientation of the grains creating the boundary.

To further confirm that inclined steps are present in the studied boundaries, their influence on single micrographs and on focal series was studied by comparing experimental data and simulations. For these calculations, simulated random grain boundaries were constructed by defining two crystals where at least one was oriented along a low index zone-axis. The step and grain boundary planes were defined as parallel to {100} and {110} planes following experimental observations [20].

For each simulated grain boundary, the sample was sectioned into thin slices and the dynamically scattered electron wave was calculated using the multi-slice approach within the EMS software package [28,29,30,31,32]. For simulated focal series, defocus values of -20nm up to 20nm were selected (at defocus steps of 2nm) whereas for simulated micrographs under negative C_s conditions Cs=-7μm, defocus=4nm were used (accelerating voltage of 300kV).

The defocus series was subsequently used to reconstruct a theoretical exit wave function using the FTSR software [16].

The influence of two inclined steps on a single micrograph is shown in Figure 7 and Figure 8. The grain on the left was oriented in the [010] zone axis and the grain on the right was randomly oriented. The segments of grain boundary plane in the viewing direction were oriented parallel to {100} planes, and inclined steps were introduced parallel to {110} planes (Figure 7e,f). One example, in which the inclined steps were parallel to two different types of planes (both {100} and {110} planes) was also studied (Figure 7c), even though this case has not been observed experimentally [20]. A boundary without inclined steps is also shown for comparison (Figure 7a). In all cases strain was not introduced in either of the grains at the boundary region. As noted in the negative Cs simulated images (Figure 8), instead of a clear transition between the crystal in the [010] zone axis and the randomly selected grain, an apparently partially disordered transition area with complex contrast appears along the boundary, although no disordered material was introduced into the simulation. This transition area is the result of the inclined steps, which change the local symmetries in the viewing direction in the vicinity of the boundary. These simulated inclined steps cause a shift in the position of segments of the grain boundary planes along the viewing direction, which is visible in the simulated images, and is similar to the contrast seen in the experimental TEM micrographs (the previously mentioned artifacts). Along the area in which the inclined steps are present, triangular shaped features appear in the simulated micrographs (marked by the dashed lines in Figure 8b), similar to those observed experimentally (Figure 5).

Increasing the number of inclined steps in a model of a boundary with higher symmetry, composed of a grain oriented in a [010] zone axis and a grain in a $\left[11\bar{2}\right]$ zone axis, resulted in

a similar transition contrast at the grain boundary (Figure 9 and Figure 10). For simplicity, both the grain boundary and the step planes along the viewing direction were set parallel to {100} planes. In this case, due to the presence of more changes between the symmetries of the delimiting grains in the beam direction, this area appear less ordered and triangular shaped patterns appear in the image in the region where the inclined steps are present.

A focal series from the boundary presented in Figure 5 was also acquired and was used to reconstruct the exit wave function using the FTSR software [16]. The phase of the exit wave function from the boundary from Figure 5 is shown in Figure 11. Nanometer length-scale steps and a partially disordered layer appear along the boundary. This area is assumed to be related to inclined steps, consistent with our data from single images. It should be noted that the disordered region at the boundary, resulting from the inclined steps, is more pronounced in the exit wave function (Figure 11) than in the single micrograph (Figure 5). To highlight this the square modulus of the Fourier transform of the phase presented in Figure 11 was filtered to remove the periodic reflections. An inverse transform was then calculated and is presented in Figure 12, enhancing regions in which non-periodic scattering is significant. From Figure 12 it can be seen that non-periodic scattering is dominant at the boundary region, due to the inclined steps.

The appearance of inclined steps was more pronounced in the exit wave function. To further confirm this, a focal series of a simulated boundary was calculated (using the boundary model in Figure 9b) and the amplitude and phase of the simulated exit wave function are presented in Figure 13. As in the experimental data, the inclined steps are more pronounced in the exit wave function rather than in a single micrograph in the simulated results (assuming negative Cs conditions as in Figure 8). It should be noted that the simulated contrast in the bulk of the

grains deviates from what would be expected for an ideally thin sample (weak phase object) due to the thickness of the simulated structure.

Discussion

Grain boundaries are usually studied using HRTEM assuming that the grain boundary is flat in the electron beam direction. Recently, grain boundaries in $SrTiO_3$ were found to have disconnections along macroscopic grain boundary planes [20]. The results presented here indicate that disconnections are also present within the thickness of TEM specimens. Here, we refer only to the step character of disconnections in the viewing direction (along the projected thickness of the TEM sample), since the dislocation component of the disconnections cannot be determined in this direction.

The presence of inclined steps in the viewing direction can appear as a "disordered" contrast at the boundary due to each inclined step resulting in the superposition of atoms from both grains in the viewing direction. This is an imaging artifact which does not exist for extremely thin edge-on grain boundaries without inclined steps. Due to the short length of the inclined steps (as expected from the experimental results involving edge-on steps reported previously [20]) and the thickness of TEM samples, it is not likely that a TEM sample without inclined steps can be produced.

Since a small number of inclined steps causes only slight changes in the contrast of TEM micrographs, this effect is not significant. Consequently, a lack of contrast resulting from inclined steps does not necessarily indicate their absence. The density of steps and the length of grain boundary planes are related to the curvature of a boundary, the orientation of the

macroscopic grain boundary plane and the orientation of the grains defining the boundary [20,26]. In addition to variations in sample thickness, the varying density of steps and lengths of grain boundary planes also affects the ratio between regions which appear ordered or disordered.

From Figure 8, slight deviations in the intensity of the step and grain boundary planes in the viewing direction are expected to appear in the boundary region when changing the orientation of the inclined steps (Figure 8b,c) or the chemical composition of the last plane of atoms (Figure 8c,d). In the case of experimental micrographs for which the quantity, chemistry and structure of the inclined steps is unknown, it is not possible to distinguish between such cases from image contrast alone. Throughout this manuscript we assume that the disconnections in the viewing direction are of a similar nature to those previously characterized along the boundary in $SrTiO_3$ [20], which was verified by simulations and experimental results. Hence, we further assume that the case presented in Figure 7c,d and Figure 8b which considers two types of inclined steps, does not occur.

The presence of inclined steps causes changes in the local effective thickness at each of the grains in the vicinity of the boundary. As a result, the contrast in HRTEM micrographs is changed, which may lead to changes in the apparent periodicity expected from bulk grains in the vicinity of the boundary. Such changes in contrast were noted in HRTEM simulations in which no distortions in the atomic structure of the grains were introduced at the boundary. In addition, in HAADF-STEM micrographs, which are less sensitive to local changes in effective thickness, the atomic structure of the bulk continued to the vicinity of the boundary where inclined steps were detected.

Summary and Conclusions

Disconnections along the viewing direction of TEM samples were found to cause an apparently disordered contrast at the grain boundary region in HRTEM micrographs. While less-ordered boundaries are possible, it was shown using image simulations that this can be an artifact, resulting entirely from inclined steps along the boundary plane which cause an overlap between the two boundary forming grains. In addition, the position of the grain boundary plane in the viewing direction can be shifted along the projected thickness of the sample by inclined steps.

Using image simulations it was shown that the density, chemistry of the last plane of atoms, and exact orientation of the inclined steps cannot be determined from the experimental data. In the work reported here it is assumed that the grain boundary and step planes in the viewing direction are of the same nature as the edge-on grain boundary and step planes along the boundary. This assumption was supported by simulations and experimental data. The resulting artifacts were found to be more pronounced in the exit wave function than in single micrographs. The appearance of inclined steps in HAADF STEM micrographs indicated an absence of structural changes at the boundary region. Therefore, changes in the local lattice structure in HRTEM micrographs at the vicinity of the boundary are caused by the presence of inclined steps and thus do not necessarily indicate the presence of strain.

Acknowledgements

This work was partially supported via a German-Israel Fund (GIF) grant No. I-1276-401.10/2014. The authors acknowledge the British Council for funding a visit by HS to the UK. AIK acknowledges the European Union under the Seventh Framework Programme under a contract for an Integrated Infrastructure Initiative Reference 312483-ESTEEM2. Financial support from EPSRC (Platform Grant EP/K032518/1) is also acknowledged.

References

1 . Lentzen M, Jahnen B, Jia CL, Thust A, Tillmann K, Urban K (2002) High-Resolution Imaging with an Aberration-Corrected Transmission Electron Microscope. Ultramicroscopy 92: 233. Doi:10.1016/s0304-3991(02)00139-0.

2. Urban KW (2008) Studying Atomic Structures by Aberration-Corrected Transmission Electron Microscopy. Science 321: 506. Doi:10.1126/science.1152800.

3. Tillmann K, Houben L, Thust A, Urban K (2006) Spherical-Aberration Correction in Tandem with the Restoration of the Exit-Plane Wavefunction: Synergetic Tools for the Imaging of Lattice Imperfections in Crystalline Solids at Atomic Resolution. J. Mater. Sci. 41: 4420. Doi:10.1007/s10853-006-0154-0.

4. Houben L (2006) Aberration-Corrected HRTEM of Defects in Strained La2CuO4 Thin Films Grown on SrTiO3. J. Mater. Sci. 41: 4413. Doi:10.1007/s10853-006-0151-3

5 . Kirkland AI, Meyer RR (2004) "Indirect" High-Resolution Transmission Electron Microscopy: Aberration Measurement and Wavefunction Reconstruction. Microscopy and Microanalysis 10: 401. Doi:10.1017/S1431927604040437.

6. Allen LJ, McBride W, O'Leary NL, Oxley MP (2004) Exit wave reconstruction at atomic resolution. Ultramicroscopy 100: 91. Doi:http://dx.doi.org/10.1016/j.ultramic.2004.01.012.

7. Haigh S, Kirkland A (2012) High Resolution Exit Wave Restoration, in Vogt T, Dahmen W, Binev P (eds), Modeling Nanoscale Imaging in Electron Microscopy, Springer US, 2012. pp. 41-72.

8. Haigh SJ, Sawada H, Takayanagi K, Kirkland AI (2010) Exceeding Conventional Resolution Limits in High-Resolution Transmission Electron Microscopy Using Tilted

Illumination and Exit-Wave Restoration. Microscopy and Microanalysis 16: 409. Doi:10.1017/S1431927610093359.

9. Kirkland AI, Saxton WO, Chau KL, Tsuno K, Kawasaki M (1995) Super-resolution by aperture synthesis: tilt series reconstruction in CTEM. Ultramicroscopy 57: 355. Doi:https://doi.org/10.1016/0304-3991(94)00191-O.

10. Kirkland AI, Saxton WO, Chand G (1997) Multiple Beam Tilt Microscopy for Super Resolved Imaging. J. Electron Microsc. 46: 11.

11. Haigh SJ, Sawada H, Kirkland AI (2009) Optimal Tilt Magnitude Determination for Aberration-Corrected Super Resolution Exit Wave Function Reconstruction. Philosophical Transactions of the Royal Society A: Mathematical, Physical and Engineering Sciences 367: 3755. Doi:10.1098/rsta.2009.0124.

12. Chang L-Y, Kirkland AI (2006) Comparisons of Linear and Nonlinear Image Restoration. Microscopy and Microanalysis 12: 469. Doi:10.1017/S1431927606060582.

13. Kirkland EJ (1982) Nonlinear High Resolution Image Processing of Conventional Transmission Electron Micrographs. Ultramicroscopy 9: 45. Doi:http://dx.doi.org/10.1016/0304-3991(82)90228-5

14. Kirkland EJ (1984) Improved High Resolution Image Processing of Bright Field Electron Micrographs. Ultramicroscopy 15: 151. Doi:http://dx.doi.org/10.1016/0304-3991(84)90037-8

15. Coene WMJ, Thust A, Op de Beeck M, Van Dyck D (1996) Maximum-Likelihood Method for Focus-Variation Image Reconstruction in High Resolution Transmission Electron Microscopy. Ultramicroscopy 64: 109. Doi:http://dx.doi.org/10.1016/0304-3991(96)00010-1

16. http://www.hremresearch.com/Eng/plugin/FTSREng.html

17. Meyer RR, Kirkland AI, Saxton WO (2002) A new method for the determination of the wave aberration function for high resolution TEM: 1. Measurement of the symmetric aberrations. Ultramicroscopy 92: 89. Doi:https://doi.org/10.1016/S0304-3991(02)00071-2

18. Meyer RR, Kirkland AI, Saxton WO (2004) A new method for the determination of the wave aberration function for high-resolution TEM.: 2. Measurement of the antisymmetric aberrations. Ultramicroscopy 99: 115. Doi:http://dx.doi.org/10.1016/j.ultramic.2003.11.001

19. Kirkland AI, Chang SL-Y, Hutchison JL. Atomic Resolution Transmission Electron Microscopy. in: Hawkes PW, Spence JCH, (Eds.). Science of Microscopy. Springer New York, New York, NY, 2007. pp. 3-64.

20. Sternlicht H, Rheinheimer W, Hoffmann MJ, Kaplan WD (2016) The Mechanism of Grain Boundary Motion in SrTiO3. J. Mater. Sci. 51: 467. Doi:10.1007/s10853-015-9058-1.

21. Rheinheimer W, Hoffmann MJ (2015) Non-Arrhenius Behavior of Grain Growth in Strontium Titanate: New Evidence for a Structural Transition of Grain Boundaries. Scr. Mater. 101: 68. Doi:http://dx.doi.org/10.1016/j.scriptamat.2015.01.021.

22. Rheinheimer W, Bäurer M, Handwerker CA, Blendell JE, Hoffmann MJ (2015) Growth of Single Crystalline Seeds into Polycrystalline Strontium Titanate: Anisotropy of the Mobility, Intrinsic Drag Effects and Kinetic Shape of Grain Boundaries. Acta Mater. 95: 111. Doi:http://dx.doi.org/10.1016/j.actamat.2015.05.019.

23. Baurer M, Kungl H, Hoffmann MJ (2009) Influence of Sr/Ti Stoichiometry on the Densification Behavior of Strontium Titanate. J. Am. Ceram. Soc. 92: 601. Doi:10.1111/j.1551-2916.2008.02920.x.

24. Rheinheimer W, Bäurer M, Chien H, Rohrer GS, Handwerker CA, Blendell JE, Hoffmann MJ (2015) The Equilibrium Crystal Shape of Strontium Titanate and its Relationship to the Grain Boundary Plane Distribution. Acta Mater. 82: 32. Doi:http://dx.doi.org/10.1016/j.actamat.2014.08.065.
25. Baram M, Kaplan WD (2008) Quantitative HRTEM Analysis of FIB Prepared Specimens. Journal of Microscopy 232: 395. Doi:10.1111/j.1365-2818.2008.02134.x.
26. Sternlicht H, Rheinheimer W, Dunin-Borkowski RE, Hoffmann MJ, Kaplan WD, Characterization of Grain Boundary Disconnections in SrTiO3 Part I: The Dislocation Component of Grain Boundary Disconnections.
27. Williams DB, Carter CB, Transmission Electron Microscopy, Springer, New York, 2009
28. Cowley JM, Moodie AF (1957) Fourier Images: I - The Point Source. Proceedings of the Physical Society. Section B 70: 486.
29. Cowley JM, Moodie AF (1957) Fourier Images: II - The Out-of-focus Patterns. Proceedings of the Physical Society. Section B 70: 497.
30. Cowley JM, Moodie AF (1957) Fourier Images: III - Finite Sources. Proceedings of the Physical Society. Section B 70: 505.
31. Cowley JM, Moodie AF (1960) Fourier Images IV: The Phase Grating. Proceedings of the Physical Society 76: 378.
32. Stadelmann PA (1987) EMS - a Software Package for Electron-Diffraction Analysis and HREM Image Simulation in Materials Science. Ultramicroscopy 21: 131. Doi:10.1016/0304-3991(87)90080-5.

Figure Captions

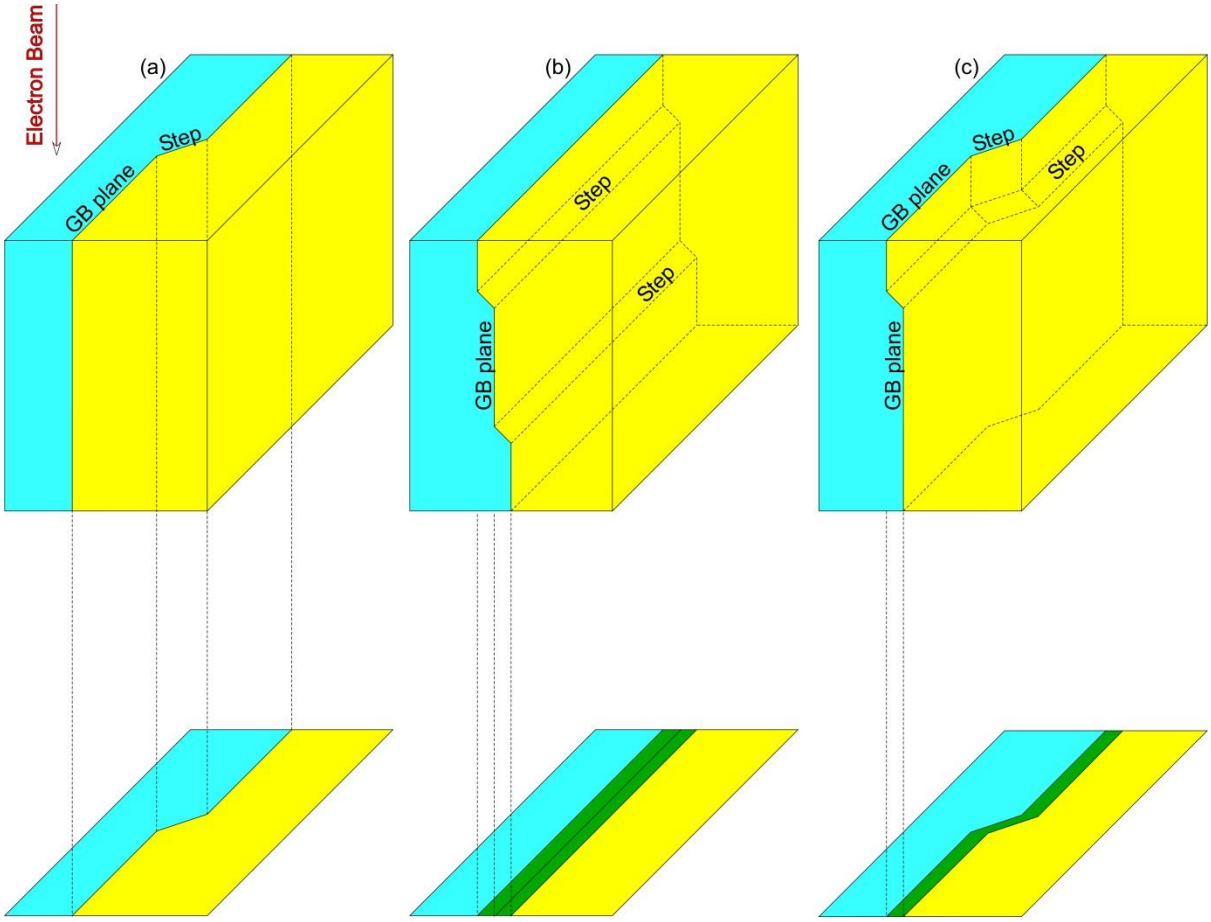

Figure 1: A schematic drawing of the definitions used in this manuscript. (a) edge-on steps and grain boundary planes are present along the boundary. (b) steps inclined to the electron beam direction are present along the boundary. The grain boundary plane in this case is parallel to the electron beam direction. (c) inclined steps intersecting with edge-on step and grain boundary planes. Below each schematic drawing of a boundary an expected representation of a TEM micrograph is shown.

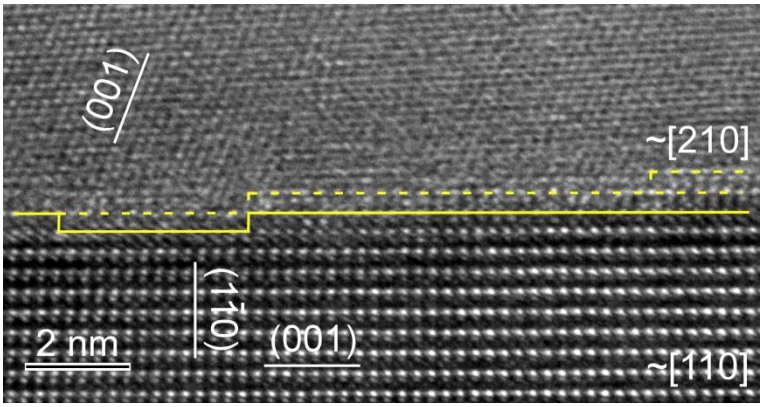

Figure 2: HRTEM micrograph of an edge-on grain boundary. The lower grain is oriented close to a [110] zone axis. The upper grain is close to a [210] zone axis. Nanometer length-scale steps are visible along the boundary. The micrograph was acquired using an accelerating voltage of 300 kV, Cs=-7.0µm, and Wiener filtered to remove noise (reproduced with permission from [20]. The difference in the overlaid markings result from dividing between edge-on and inclined steps in this work).

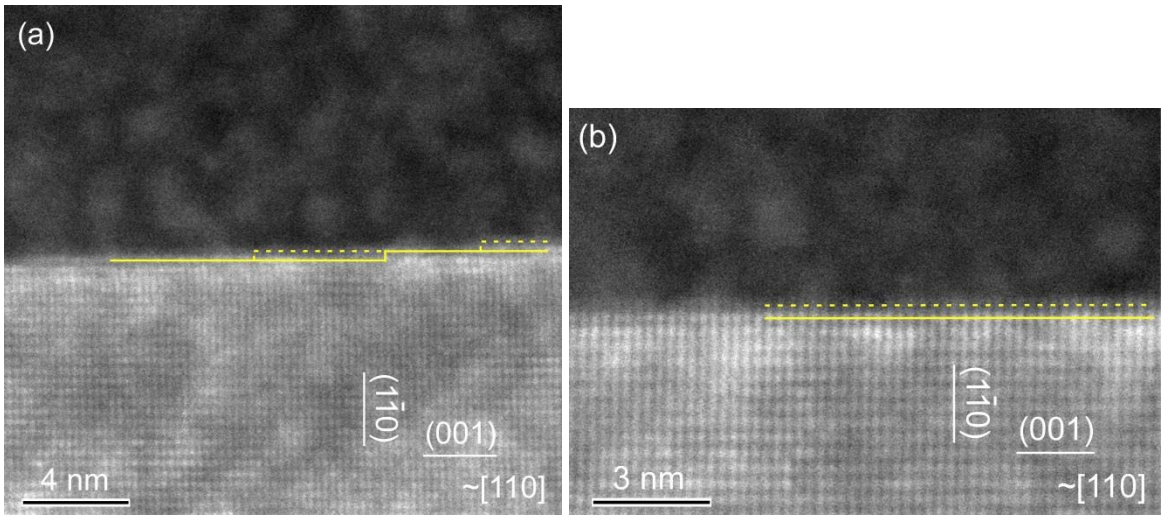

Figure 3: HAADF STEM micrographs of the grain boundary presented in Figure 2. The micrograph was acquired using an accelerating voltage of 300 kV.

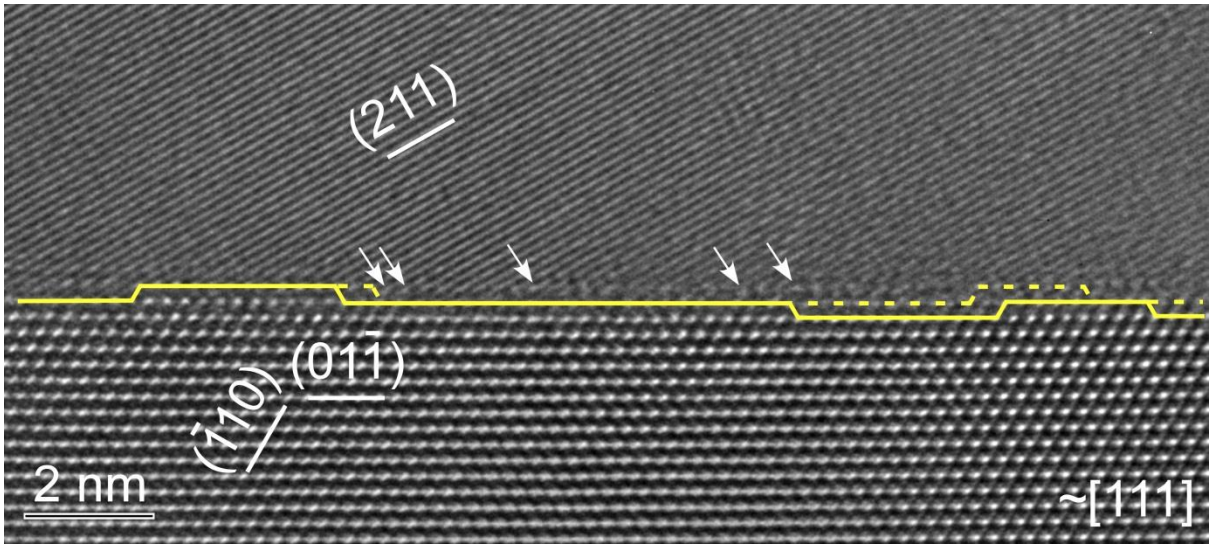

Figure 4: HRTEM micrograph of an edge-on grain boundary. The lower grain is oriented close to a [111] zone axis. Nanometer length-scale steps are visible along the boundary. The micrograph was acquired using an accelerating voltage of 300kV, Cs=-7.0µm, and Wiener filtered to remove noise (reproduced with permission from [20]. The difference in the overlaid markings result from dividing between edge-on and inclined steps in this work).

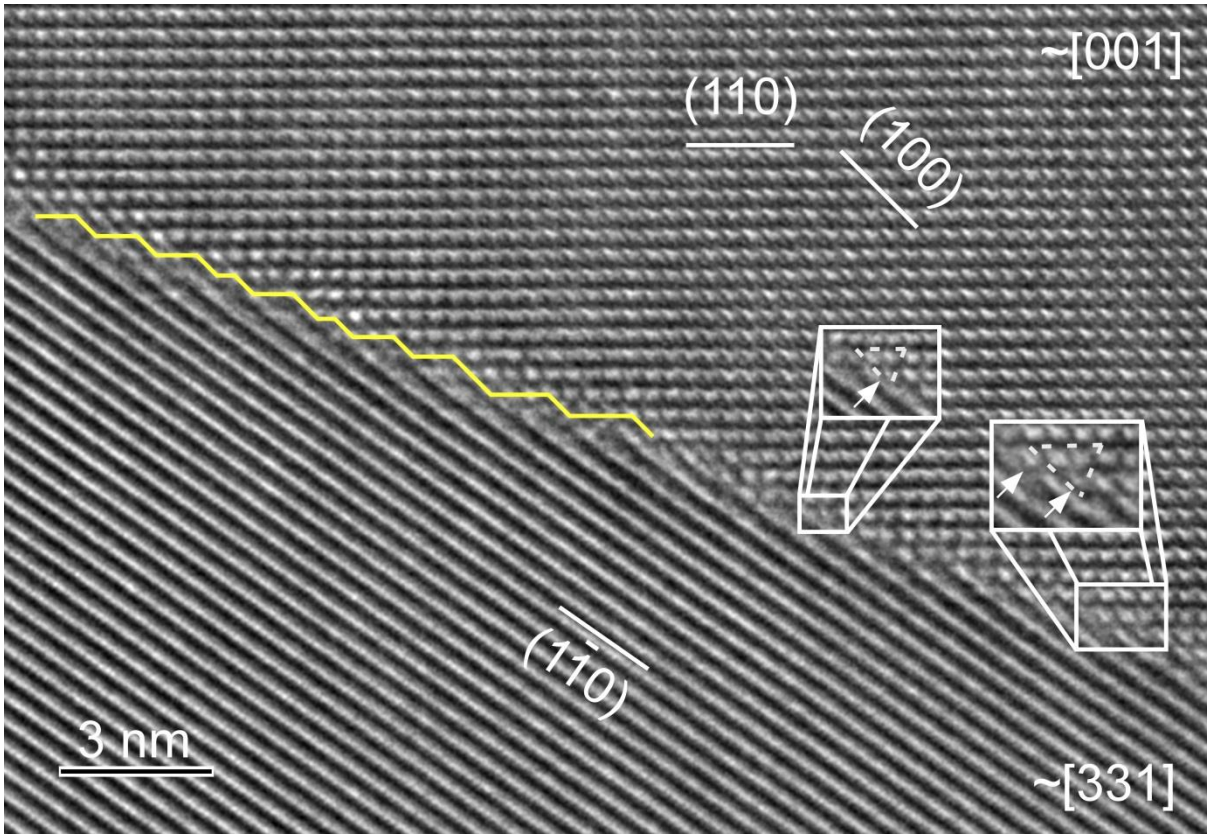

Figure 5: HRTEM micrograph of an edge-on general grain boundary. The upper grain is oriented close to a [001] zone axis. Nanometer length-scale steps are visible along the boundary (marked in yellow). The lower grain is close to a [331] zone axis. The micrograph was acquired using an accelerating voltage of 300kV, Cs =-5.69 μm, and Wiener filtered to remove noise (reproduced with permission from [20]).

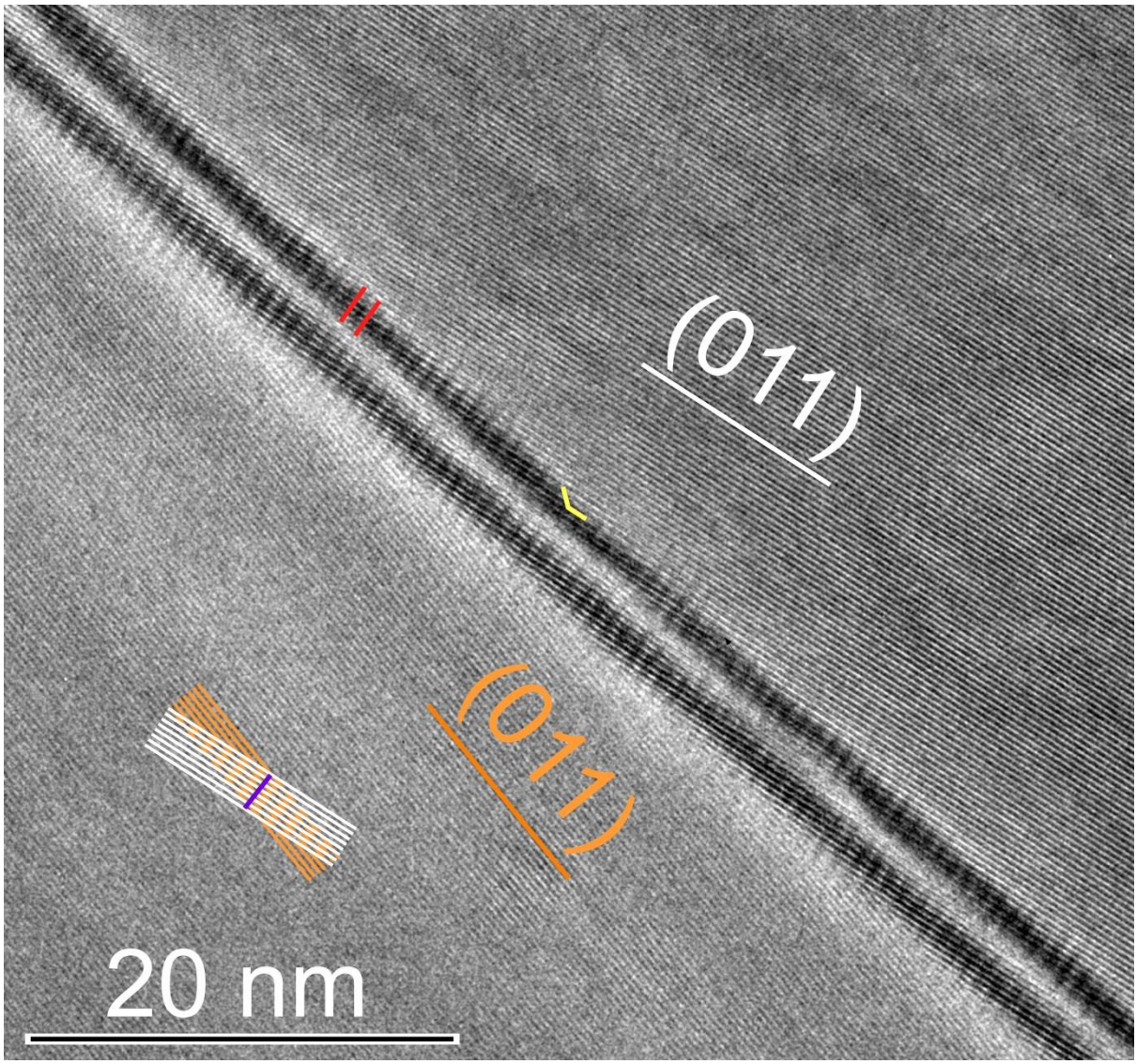

Figure 6: HRTEM micrograph of a tilted boundary. The red lines indicate a Moiré pattern. The white and orange lines indicate the periodicity of the (011) planes of the upper and lower grains respectively. The purple line indicates the Moiré pattern resulting from the white and orange lines. The yellow lines indicate estimated grain boundary and step planes. The

micrograph was acquired using an accelerating voltage of 300kV, Cs=-7.6μm, and Wiener filtered to remove noise.

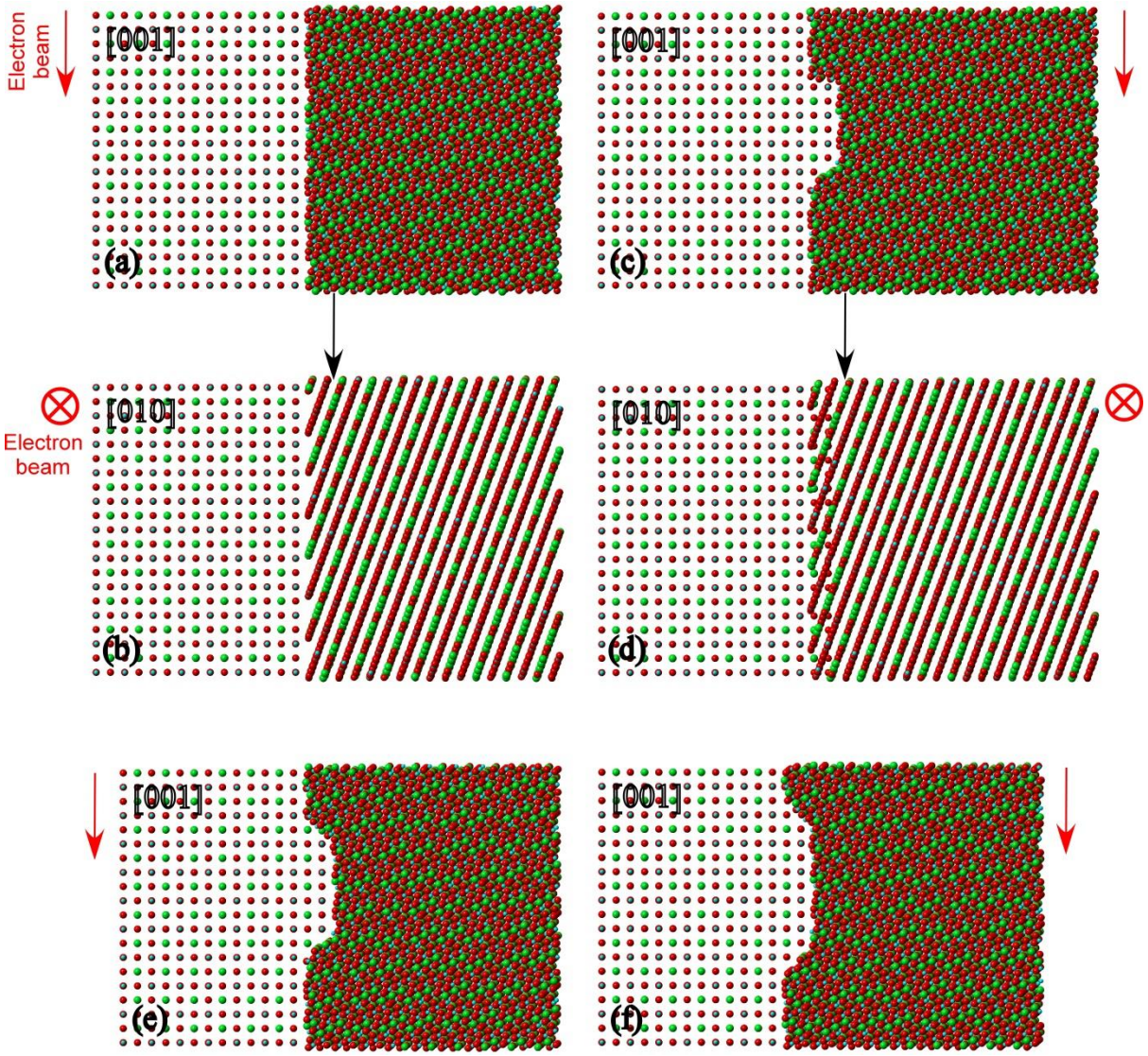

Figure 7: Boundary models with and without inclined steps. In (a,c,e,f) the grain on the left is oriented along [001] zone axis. (b,d) were constructed by tilting the boundaries in (a,c) by 90° respectively. (a and b, c and d, e,f) were used to create the simulated images in Figure 8. (a,b) A flat grain boundary without steps. (c,d) A grain boundary with two steps along {001} and {110} planes. (e) A grain boundary with two steps, both along {110} planes. TiO-Sr terminations were selected along {110} planes. (f) A grain boundary with two steps, both along {110} planes. O-O terminations were selected along {110} planes. The electron beam

direction is marked in red in all diagrams. Green circles represent Sr, red represents O and blue represents Ti.

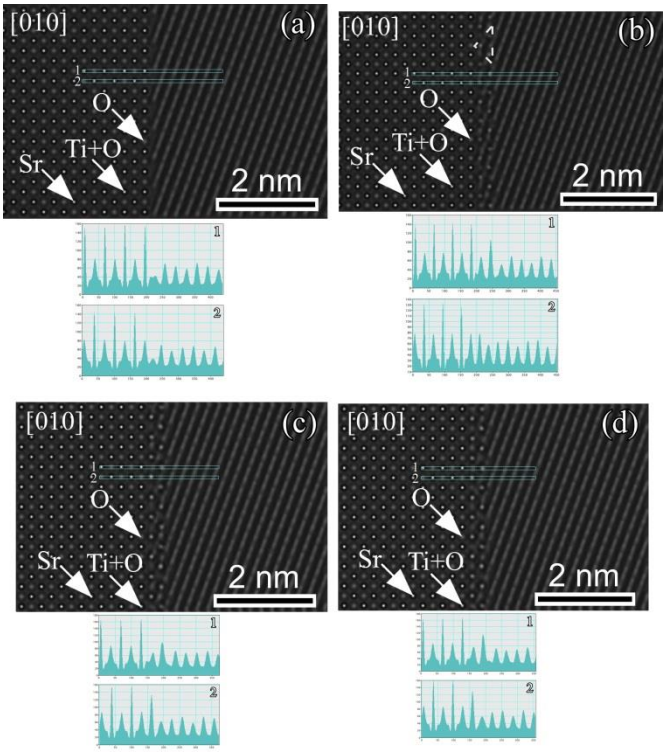

Figure 8: Simulated HRTEM images of boundaries where the majority of the boundary is edge-on under negative Cs imaging conditions (Cs=-7μm, defocus=4nm, accelerating voltage of 300kV). The images were simulated based on the boundary models presented in Figure 7. The grain on the left is oriented along [010] zone axis. (a) A flat edge-on grain boundary without steps (Figure 7 a and b). (b) A grain boundary with two inclined steps along {001} and {110} planes (Figure 7 c and d). (c) A grain boundary with two inclined steps, both along {110} planes. TiO-Sr terminations were selected along {110} planes (Figure 7 e). (d) A grain boundary with two inclined steps, both along {110} planes. O-O terminations are along {110} planes (Figure 7 f).

Figure 9: (a) Boundary model with 21 inclined steps. The grain on the left is oriented along [001] zone axis and the grain on the right is oriented along [111] zone axis. (b) The boundary after rotating (a) by 90° to the orientation used to simulate the image in Figure 10. The

electron beam direction is marked in red. Green circles represent Sr, red represents O and blue represents Ti.

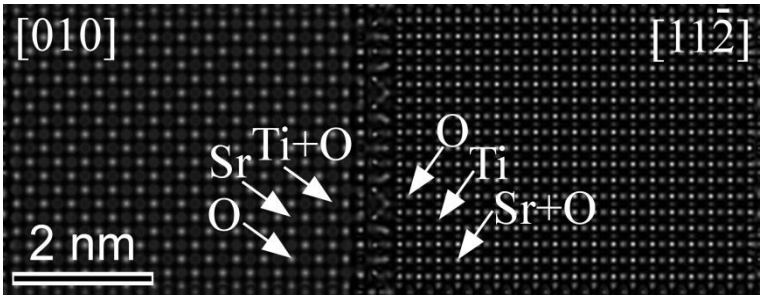

Figure 10: Simulated HRTEM image of an edge-on grain boundary (Figure 9b) under negative Cs imaging conditions with inclined steps (Cs=-7μm, defocus=4nm, accelerating voltage of 300kV). The left grain is oriented along [010] zone axis and the right grain along $\left[11\bar{2}\right]$ zone axis.

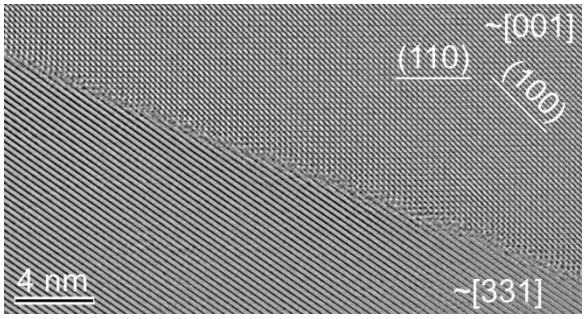

Figure 11: Experimentally recovered phase of the exit wave function of the GB presented in Figure 5. Nanometer length-scale steps are visible along the boundary and a partially disordered layer is evident.

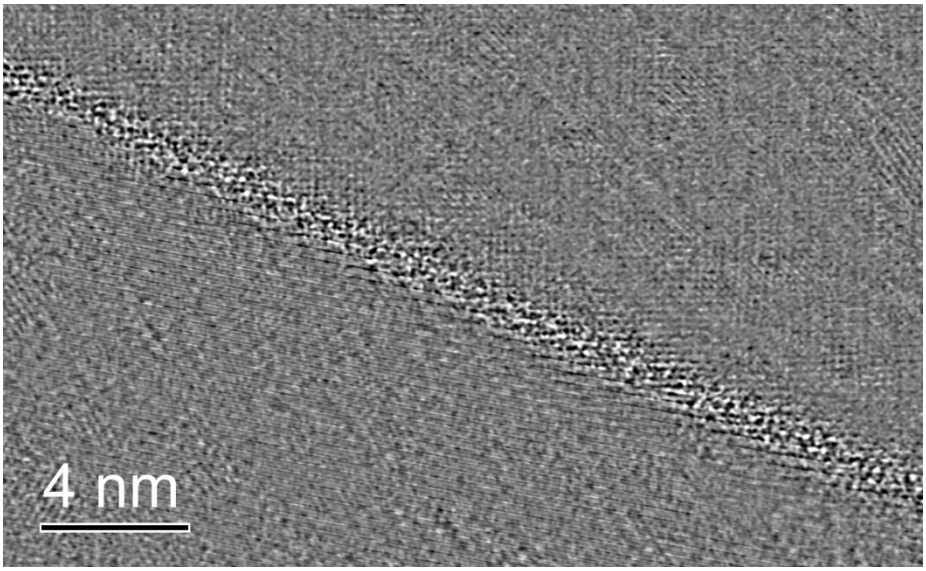

Figure 12: An inverse transform of a filtered Fourier transform of the phase presented in Figure 11, highlighting regions in which non-periodic scattering is dominant.

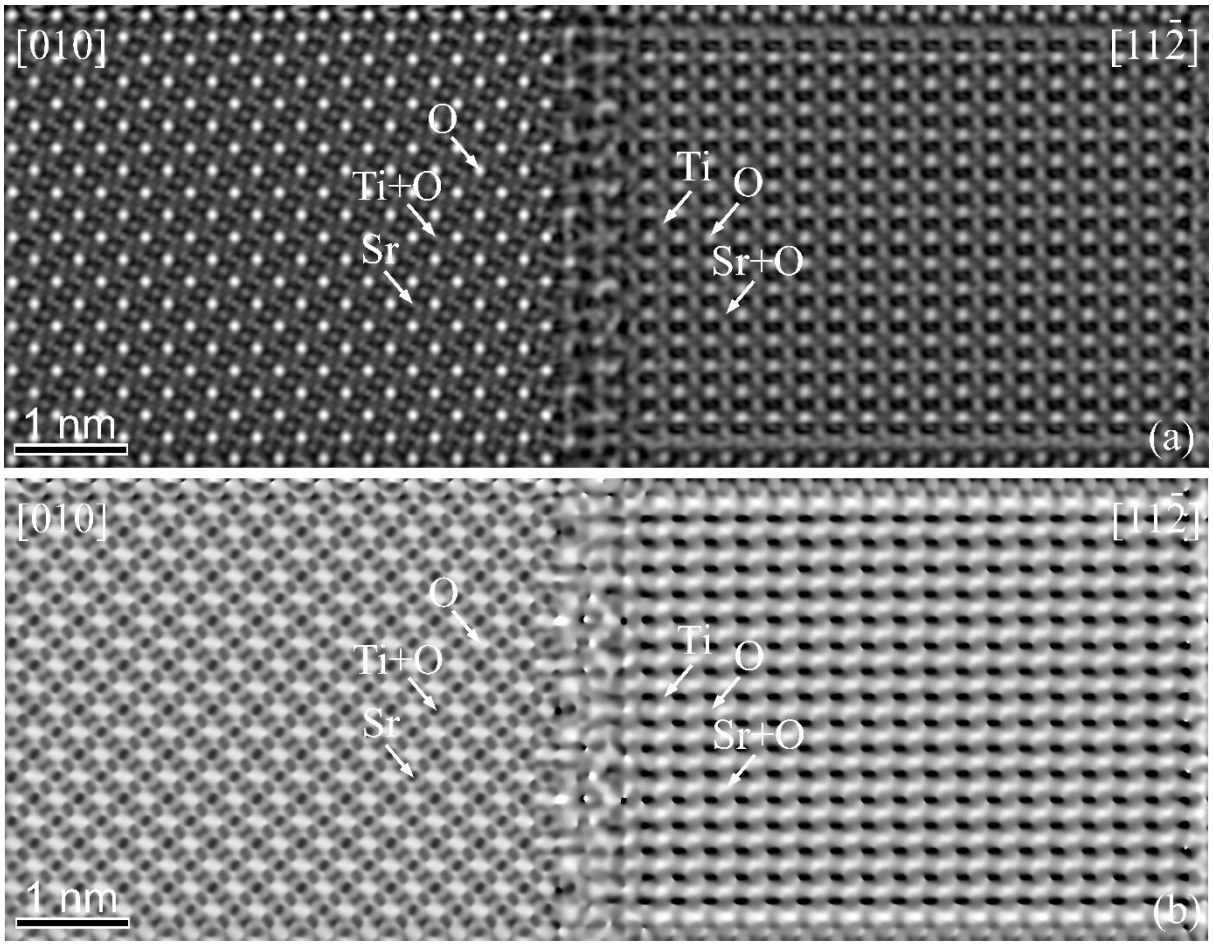

Figure 13: (a) Amplitude and (b) phase of the exit wave function of the boundary presented in Figure 9b.